J Biomol NMR (2017) 68:33–39
DOI 10.1007/s10858-017-0112-y

ARTICLE

Comparison of the free and ligand-bound imino hydrogen exchange rates for the cocaine-binding aptamer

Zachary R. Churcher[1] · Miguel A. D. Neves[1,2] · Howard N. Hunter[1] · Philip E. Johnson[1]

Received: 21 December 2016 / Accepted: 28 April 2017 / Published online: 5 May 2017

Abstract Using NMR magnetization transfer experiments, the hydrogen exchange rate constants (k_{ex}) of the DNA imino protons in the cocaine-binding aptamer have been determined for the free, cocaine-bound, and quinine-bound states. The secondary structure of the cocaine-binding aptamer is composed of three stems built around a three-way junction. In the free aptamer the slowest exchanging imino protons are located in the middle of the stems. The highest k_{ex} values were found for a nucleotide in the GAA loop of stem 3 and for nucleotides at the end of the stems that form the three-way junction structure and in the tandem GA mismatch. Upon ligand binding, the k_{ex} values of nucleotides at the ligand binding site are reduced, indicating that these base pairs become more stable or less solvent accessible in the bound state. The imino proton k_{ex} values of nucleotides located away from the binding site are only minimally affected by ligand binding.

Keywords Aptamer function · Hydrogen exchange rate constant · Ligand binding · DNA-small molecule interactions

Electronic supplementary material The online version of this article (doi:10.1007/s10858-017-0112-y) contains supplementary material, which is available to authorized users.

✉ Philip E. Johnson
pjohnson@yorku.ca

[1] Department of Chemistry and Centre for Research on Biomolecular Interactions, York University, Toronto, ON M3J 1P3, Canada

[2] Present Address: Department of Laboratory Medicine, Keenan Research Centre for Biomedical Science, St. Michael's Hospital, Toronto, ON M5B 1W8, Canada

Introduction

Aptamers are nucleic acid molecules that have been selected to bind a particular ligand that can range from a small molecule to a cell. Aptamers typically bind with high affinity and selectivity, and they have been found to be useful in medical and analytical applications (Cho et al. 2009; Vinkenborg et al. 2011; Mascini et al. 2012; Kim et al. 2016; Ilgu and Nilsen-Hamilton 2016). Understanding how aptamers interact with their ligands is an important question when implementing an aptamer in a biotechnology application. Measuring the hydrogen exchange rate constant (k_{ex}) for the imino proton of free and ligand-bound aptamers is a useful probe of how base pair dynamics change with ligand binding, as this exchange rate reflects the stability and solvent accessibility of base pairs (Guéron and Leroy 1995). The hydrogen exchange rate constant in nucleic acids is measured using water magnetization transfer experiments and has been previously employed in studying both DNA and RNA duplex and aptamer molecules (Nonin et al. 1997; Nonin-Lecomte et al. 2001; Lee and Pardi 2007; Lee et al. 2008, 2012).

The cocaine-binding aptamer is a widely used model system for studying aptamer function and biotechnology applications of aptamers (Baker et al. 2006; Sharma and Heemstra 2011; Roncancio et al. 2014; Neves et al. 2015; Sachan et al. 2016; Grytz et al. 2016; Harkness et al. 2016). The aptamer was originally selected by Stojanovic et al. (2000, 2001) to bind cocaine, but not any of the common cocaine metabolites. Unusually, this aptamer binds quinine 50-fold tighter than cocaine (Pei et al. 2009; Reinstein et al. 2013; Slavkovic et al. 2015). Structurally, the cocaine-binding DNA aptamer consists of three stems centered around a three-way junction (Neves et al. 2010b). The two variants of the cocaine-binding

aptamer studied here are MN4 and MN19 (Fig. 1). MN4 is a sequence variant of the originally reported cocaine-binding aptamer that binds more tightly to cocaine, while MN19 is a variant of MN4, where the length of stem 1 has been reduced to three base pairs. The MN19 aptamer is most commonly utilized in biotechnology applications, as it has a ligand-induced folding mechanism. In the unbound state, MN19 is poorly structured or unstructured, and the aptamer becomes folded concurrently with ligand binding (Stojanovic et al. 2001; Neves et al. 2010b).

In this study, we measure the k_{ex} values of the imino protons in both the MN4 and MN19 aptamers in their free, cocaine-bound, and quinine-bound states. We find that base pairs at the ligand-binding site have reduced k_{ex} values in both their quinine and cocaine-bound forms. The k_{ex} values of nucleotides away from the binding site are minimally affected by ligand binding suggesting a decrease in base pair dynamics at the binding site is occurring, but that a reduction in k_{ex} values is not felt throughout the molecule.

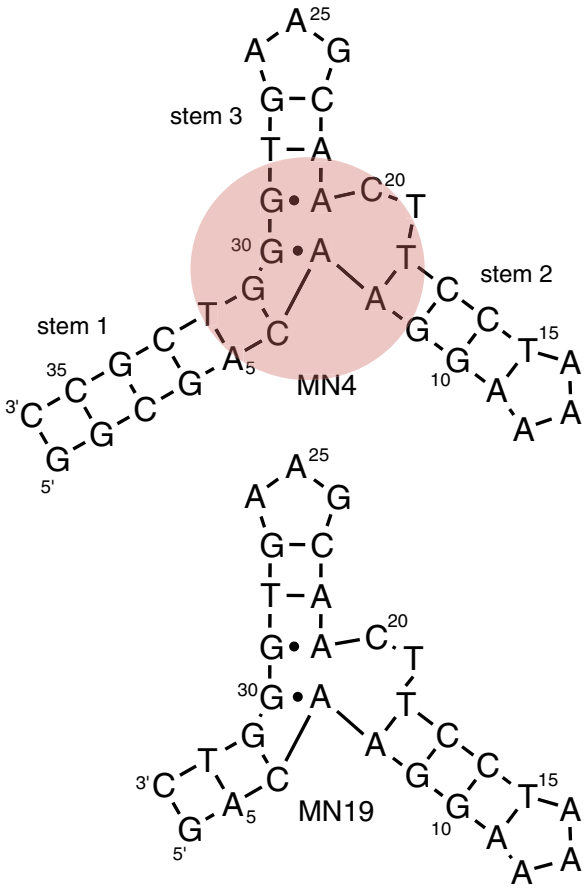

Fig. 1 Secondary structure of the MN4 and MN19 cocaine-binding aptamers used in this study. For ease of comparison both aptamers follow the same numbering scheme. Highlighted in MN4 is the location of the high affinity ligand-binding site

Materials and methods

Materials

All DNA samples were obtained from Integrated DNA Technologies (IDT) as a dry powder. DNA samples were exchanged against 1 M NaCl three times, and then exchanged against deionized water four times. Aptamer samples were reduced to 1000 µL in volume and then the concentration was determined using UV–Vis spectroscopy on a Varian Cary 100 Bio UV–Vis spectrophotometer by measuring the A_{260} and using the extinction coefficient provided by IDT. Quinine hemisulfate monohydrate was obtained from Sigma–Aldrich (Catalog No. 145912). Stock solutions were prepared by dissolving an appropriate amount of quinine hemisulfate monohydrate in water. Cocaine hydrochloride was obtained from Sigma–Aldrich (Catalog No. C-5776), and cocaine samples were prepared from a 0.5 M stock solution of cocaine hydrochloride.

NMR experiments

NMR experiments were conducted on a 600 MHz Bruker DRX Avance spectrophotometer equipped with a ^{1}H–^{13}C–^{15}N triple-resonance probe at 5 °C. Samples were heated and cooled to favor intramolecular folding of the aptamers prior to performing NMR experiments. Spectra were acquired in 10% $^{2}H_2O$, 90% H_2O. These conditions were based on our previous studies in which no added NaCl produced spectra with the best signal to noise ratio (Neves et al. 2010a). NMR data were processed using XWIN-NMR 3.5 (Bruker) and spectra were analysed using Mestrenova version 11.0. For both the MN4 and MN19 aptamers the original sample was divided in half before the NMR data for the free aptamer was acquired. Then cocaine was titrated in until a 1:1 complex was obtained using our previously published titrations as a guide (Neves et al. 2010b). With the second half of the aptamer sample, quinine was titrated in to form a 1:1 complex, again, using our previous titrations as a guide (Reinstein et al. 2013). Sample volumes were from 550 to 600 µL, and concentrations of all samples of both MN4 and MN19 aptamers were 1.0 mM.

The imino hydrogen exchange rates were determined as outlined by the method of Lee and Pardi (2007). The apparent relaxation constant of water (R_{1w}), and the apparent relaxation constant of each imino proton (R_{1a}) was determined using a selective inversion recovery experiment employing a 180° shaped pulse to select either water

or the imino region of the spectrum as appropriate. The peak intensities of the imino protons were measured using a water magnetization transfer experiment, using a 180° shaped pulse along the imino region. Twenty experiments were acquired using delay times of 5–100 ms.

Data analysis

The R_{1w} and R_{1a} values were obtained by measuring the intensity of either the water or imino peaks in the inversion recovery spectra and fitting the intensities to a single exponential curve. The intensities of the resonances in the magnetization transfer experiments were then measured and the data were fit to Eq. 1 using the Sigma Plot 11 software package (Systat Software) (Lee and Pardi 2007; Lee et al. 2008):

$$\frac{I(t)}{I_0} - 1 = -2\frac{k_{ex}}{R_{1w} - R_{1a}}\left(e^{-R_{1a}t} - e^{-R_{1w}t}\right) \quad (1)$$

where $I(t)$ is the peak intensity as a function of delay time, I_o is the peak intensity with a delay time of 0 s, R_{1w} is the apparent relaxation rate constant of water, R_{1a} is the apparent relaxation rate constant of a particular nucleotide, k_{ex} is the exchange rate constant for the nucleotide, and t is the delay time in seconds. Once the constants (R_{1w} and R_{1a}) for the equation were obtained, k_{ex} was determined by rearranging Eq. 1 to isolate for k_{ex}.

Results and discussion

NMR spectroscopy

Resonance assignments for the imino regions of both MN4 and MN19, free, cocaine-bound and quinine-bound states were obtained based on our previous studies (Fig. 2) (Reinstein et al. 2013; Neves et al. 2010b). The spectra reported here are very similar to what we reported previously.

Imino resonance intensity was measured as a function of time using semi-selective inversion recovery experiments for both MN4 and MN19 in their free, cocaine-bound and quinine-bound states. Due to peak overlap we were not able to independently measure the intensity of every imino or even the same imino resonances in different aptamer states. For example, G4, G9, G10 and G27 all overlap together or with another resonance in this group, except for cocaine-bound MN4, where G4 appears as a separate resonance (Fig. 2). We were able to measure the intensity of ten different imino resonances from the 15-guanine and thymine nucleotides in MN4 (not including G1). Of these ten, we are able to measure the exchange rate constant from six

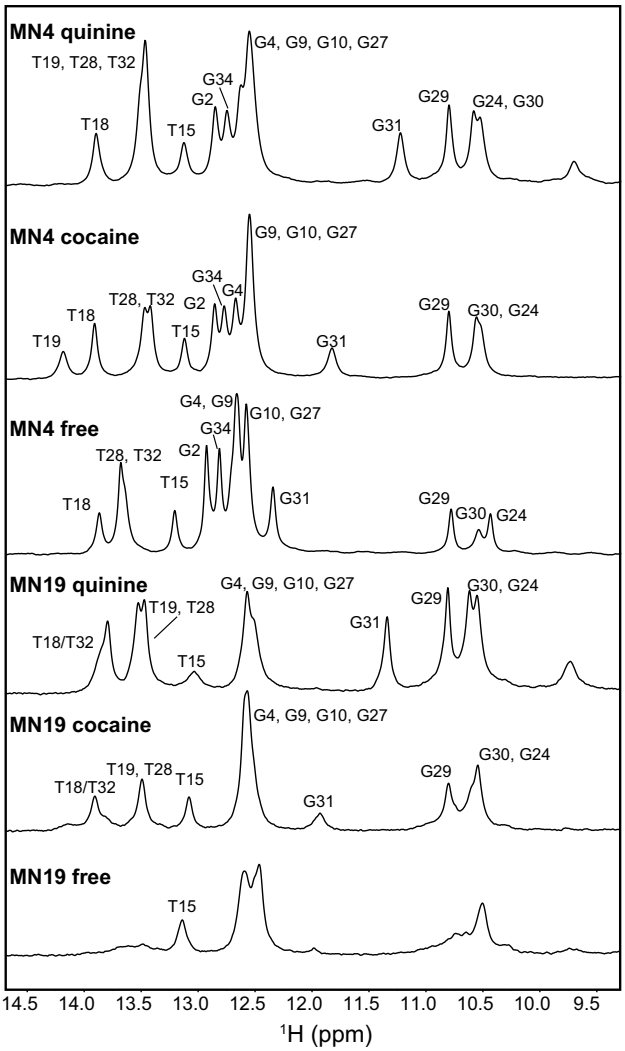

Fig. 2 Downfield imino region of the 1D-^{1}H NMR spectra of MN4 and MN19 cocaine-binding aptamers free and bound to cocaine and quinine. Spectra were acquired at 5 °C in 10% ^2H_2O, 90% H_2O

different nucleotides in the free, cocaine-bound and quinine-bound states.

We obtained 20 1D spectra at different delay times in order to fit the intensity decay and obtain k_{ex} values. Figure 3a shows ten selected spectra of the MN4 cocaine-bound state. Fast decaying nucleotides such as T15 produce a negative signal by the last decay time while slower decaying signals (T19, G29) still have a positive intensity with the same delay time. An example decay curve, used to obtain k_{ex} for G29 in MN4, is displayed in Fig. 3b. For this nucleotide, the imino resonance in the free state decays to a greater degree than in the quinine and cocaine-bound states. The two bound states decay in a similar manner. The error in the normalized peak intensity in the decay curve was obtained from measuring the peak height in two separate experiments and obtaining a standard deviation. The

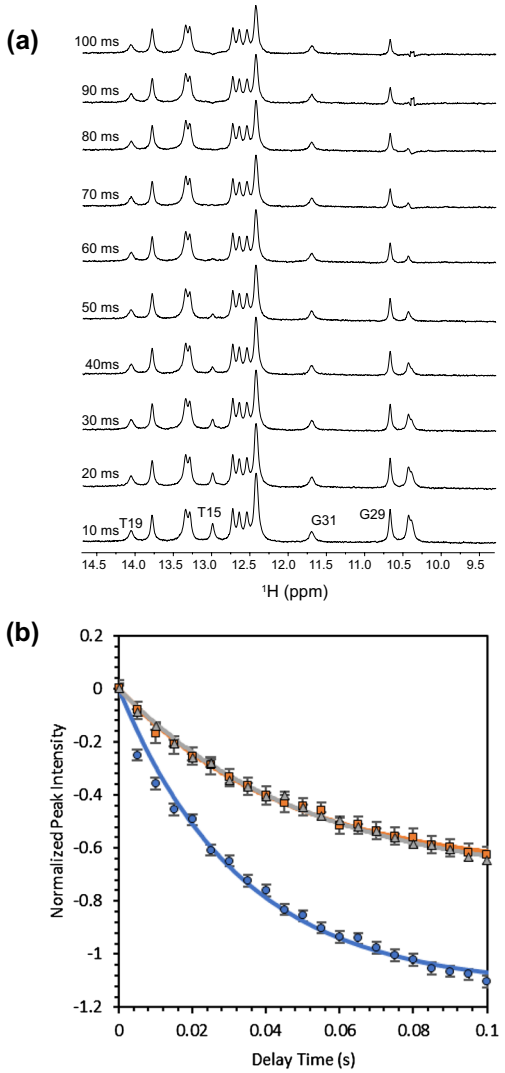

Fig. 3 **a** 1D spectra of the water magnetization transfer experiment for the imino protons in the MN4 bound to cocaine sample. Delay times range from 10 to 100 ms. Selected nucleotides are numbered. **b** Intensity of the G29 imino resonance as a function of delay time. *Blue circles* are from free MN4, *grey triangles* are from the quinine-bound MN4 and *orange squares* are from the cocaine-bound MN4. The *line* represents the best fit to Eq. 1. The intensities are normalized

error bars in Fig. 3b represent the standard deviation of the measurement. Decay curves for all measured peaks are shown in the Supporting Material. In general the data presented in Fig. 3b and in the Supporting Material agree with Eq. 1 producing an average R^2 value of 0.96 with a range of 0.81–0.99. Exchange rate constants for MN4 and MN19 are given in Table 1.

Hydrogen exchange rate constants

The values of hydrogen exchange rate constants of the imino protons in the MN4 aptamer reflect the position of the nucleotide in the secondary structure of the aptamer (Fig. 1; Table 1). In the free MN4 aptamer the nucleotides with the lowest exchange rate constants are G2 and G34 with k_{ex} values of (1.9 ± 0.6) and (2.2 ± 0.6) s^{-1}, respectively, and are located in the middle of a stem. The nucleotide with the largest exchange rate constant is G24 (36.3 ± 8.5) s^{-1}, and it is located in the loop of stem 3. Between these extremes are G29 and G30, the guanine residues that comprise the tandem GA mismatch (k_{ex} values of (17.0 ± 2.1) and (21.8 ± 3.2) s^{-1}, respectively), and residues located at the end of stems such as T15 (12.8 ± 1.3), T18 (7.5 ± 1.6) and G31 (12.7 ± 1.8) s^{-1}.

The hydrogen exchange rates of the imino protons were analysed in order to determine the effect of ligand binding at the individual base pair level. For resonances whose k_{ex} values were measured in more than one state, the values are shown graphically in Fig. 4, and their percent increase or decrease are depicted in Fig. 5. With cocaine binding T18, G29 and G31 display a large reduction in k_{ex} values. These three nucleotides are located at the MN4 high affinity binding site. The cocaine-binding aptamer has two ligand binding sites, a high affinity site involving nucleotides at the three-way junction and the end of stem 1 abutting the three-way junction. A second, lower affinity site mostly involves nucleotides located in stem 2 (Neves et al. 2017). In this study, given the amount of ligand added and the K_d difference between the two sites, we are only significantly populating the high affinity site.

In contrast to the reduction in k_{ex} for nucleotides at the high affinity site, the k_{ex} value of T15, located away from the high affinity binding site at the end of stem 2, is unchanged with cocaine binding and remains high at (12.8 ± 1.3) s^{-1} in the free and (13.5 ± 0.8) s^{-1} in the cocaine-bound states. The k_{ex} values of G2 and G34, also located away from the binding site are unchanged and remain low when cocaine-bound. We will also note that for T19, which is at the centre of the high-affinity binding site, and only observed as an isolated peak in the cocaine-bound MN4 complex, the k_{ex} value is low (2.7 ± 2.0) s^{-1} and within the uncertainty range for its adjacent nucleotide T18 despite it being in the dinucleotide bulge (Fig. 1). Finally, we are able to measure the k_{ex} value for G4 in the cocaine-bound MN4 complex to be (4.3 ± 0.7) s^{-1}. This value is slightly higher than the nucleotides G2 and G34 in stem 1, but certainly not a fast-exchanging residue.

The effects of quinine binding on the k_{ex} values of MN4 are similar to what we see with cocaine binding (Table 1; Fig. 4). All the k_{ex} values that can be measured in both bound states are within the error range of each other, with the exception of T15. The nucleotides T18, G29 and G31, are located at the high-affinity site that experience a significantly decreased k_{ex} value for cocaine binding, display an analogous behavior when quinine is bound. The k_{ex}

Table 1 Hydrogen exchange rate constants (s^{-1}) of the imino protons for the free and bound MN4 and MN19 aptamers

Residue	MN4			MN19		
	Free	Cocaine	Quinine	Free	Cocaine	Quinine
G2	1.9 ± 0.6	2.3 ± 0.8	3.6 ± 0.6	–	–	–
G4	–	4.3 ± 0.7	–	–	–	–
T15	12.8 ± 1.3	13.5 ± 0.8	18.2 ± 2.5	18.2 ± 2.5	18.6 ± 3.6	19.1 ± 4.7
T18	7.5 ± 1.6	3.0 ± 0.9	1.1 ± 0.9	–	–	–
T19	–	2.7 ± 2.0	–	–	–	–
G24	36.3 ± 8.5	–	–	–	–	–
G29	17.0 ± 2.1	7.5 ± 0.8	7.2 ± 0.9	–	14.5 ± 1.6	8.9 ± 1.3
G30	21.8 ± 3.2	–	–	–	–	–
G31	12.7 ± 1.8	2.1 ± 1.9	3.5 ± 1.2	–	20.1 ± 3.3	4.7 ± 1.3
G34	2.2 ± 0.6	2.7 ± 0.6	2.9 ± 0.7	–	–	–

All data acquired at 5 °C in 10% ^2H_2O, 90% H_2O. The uncertainty represents the error in the fit of the data

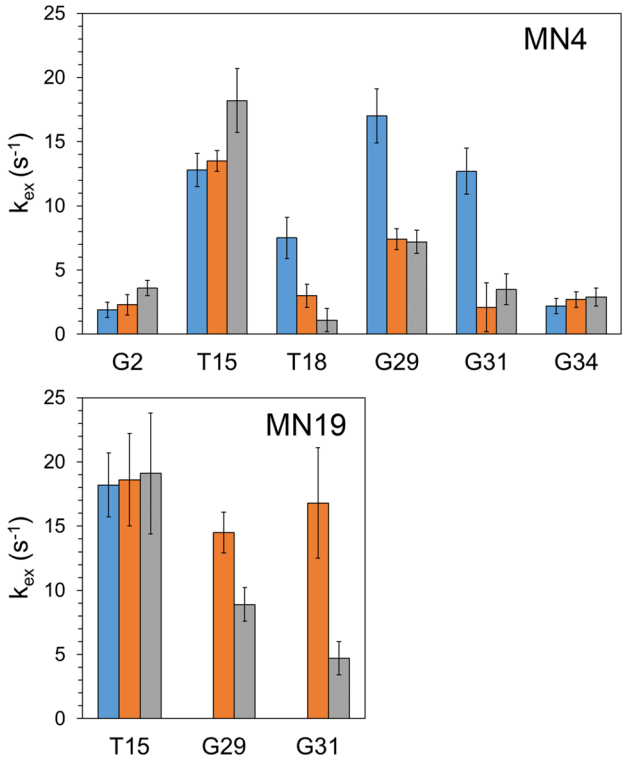

Fig. 4 Comparison of the imino exchange rates in MN4 (*top*) and MN19 (*bottom*). In *blue* are data for free aptamer, in *orange* are data for cocaine-bound aptamer, and in *grey* are data for the quinine-bound aptamer. Only nucleotides with data from more than one state are shown

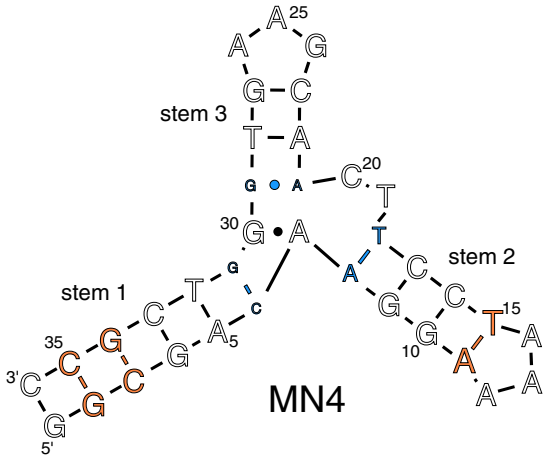

Fig. 5 Change in imino exchange rate with ligand binding mapped onto the MN4 secondary structure. *Blue* corresponds to a reduction in the imino exchange rate with ligand binding with the magnitude of change represented by a decrease in font size. *Orange* corresponds to an increase in the imino exchange rate with ligand binding with the magnitude of change represented by an increase in font size. Residues for which we do not have data in the free state and both bound states are in *outlined black lettering*

value of T15 remains high when quinine is bound and even increases significantly compared to the free and cocaine-bound states though only slightly greater than the uncertainty in the values.

For MN19, our data set is very limited due to overlapping signals. In the free state, MN19 is thought to be loosely structured or unfolded (Stojanovic et al. 2001; Reinstein et al. 2013; Neves et al. 2010b) and of the approximately five imino protons detected we are only able to assign the imino of T15 (Fig. 2). In the cocaine and quinine-bound states, the expected number of imino protons for the MN19 secondary structure shown in Fig. 1 are detected. However, we are only are able to measure the k_{ex} for the imino resonances of G29 and G31 in addition to T15 due to signal overlap. The k_{ex} values of T15 are similar in all three states of MN19 (Fig. 4; Table 1). For G29 and G31, both residues are at the high affinity site, the k_{ex} values are lower in the quinine-bound state than the cocaine-bound state, possibly, reflecting the higher affinity of MN19 for quinine. For both nucleotides, the k_{ex} values are higher in MN19 than we observed in

MN4 indicating that this aptamer is more dynamic than MN4 and consistent with MN19 having a lower melting point (T_m) than MN4 in both the cocaine and quinine-bounds forms (Harkness et al. 2016).

The reduction in k_{ex} values with ligand binding we observe here for residues at the ligand-binding site is consistent with previous aptamer-ligand studies. A free aptamer versus protein-bound aptamer study of the macugen-$VEGF_{165}$ interaction showed that the free aptamer had many residues whose imino protons were not observed due to a high exchange rate in the free state. In the bound state, many of these protons were observable and the k_{ex} values were less than 1.5 s^{-1} (Lee et al. 2008). In our case, even with the binding of a small organic molecule, we also see a reduction in k_{ex} values at the ligand-binding site. Other studies on riboswitches, though not involving measuring k_{ex} rates but instead small-angle X-ray scattering (SAXS) based studies, have also shown that many riboswitches can become compact with ligand binding. However, this phenomenon is not observed in all cases (Zhang et al. 2014). In MN4, the tandem GA mismatch at the three-way junction has a lower k_{ex} rate in the ligand-bound forms than in the free state. This reduction in mobility might be necessary for binding given than the replacement of the G29-A21 base pair with a GC base pair greatly reduces cocaine affinity (Green et al. 2006; Reinstein et al. 2011) though structural changes may also play a role.

Conclusions

Using magnetization transfer experiments the k_{ex} values of imino protons in the MN4 and MN19 cocaine-binding aptamers have been measured in the free, cocaine-bound and quinine-bound states. With ligand binding we observe a significant reduction in the k_{ex} values for nucleotides T18, G29 and G31 located at the binding site in the aptamer. We see only minor changes in the k_{ex} values of imino protons located away from the binding site. This trend we observe, of a reduction of imino proton k_{ex} values at the binding site upon ligand binding has been seen before in the macugen-$VEGF_{165}$ complex (Lee et al. 2008), the AMP-RNA aptamer complex (Nonin et al. 1997) and the AMP-DNA aptamer complex (Nonin-Lecomte et al. 2001) and appears to be a general feature in aptamer-ligand interactions.

Acknowledgements We thank members of the Johnson lab (York University, Toronto) for useful discussions. This work was supported by funding from the Natural Sciences and Engineering Research Council of Canada (NSERC) to P.E.J.

References

Baker BR, Lai RY, Wood MS, Doctor EH, Heeger AJ, Plaxco KW (2006) An electronic, aptamer-based small-molecule sensor for the rapid, label-free detection of cocaine in adulterated samples and biological fluids. J Am Chem Soc 128:3138–3139

Cho EJ, Lee J-W, Ellington AD (2009) Applications of aptamers as sensors. Annu Rev Anal Chem 2:241–264

Green E, Olah MJ, Abramova T, Williams LR, Stefanovic D, Worgall T, Stojanovic MN (2006) A rational approach to minimal high-resolution cross-reactive arrays. J Am Chem Soc 128:15278–15282

Grytz CM, Marko A, Cekan P, Sigurdsson ST, Prisner TF (2016) Flexibility and conformation of the cocaine aptamer studied by PELDOR. Phys Chem Chem Phys 18:2993–3002

Guéron M, Leroy J-L (1995) Studies of base pair kinetics by NMR measurement of proton exchange. Methods Enzymol 261:383–413

Harkness RW, Slavkovic S, Johnson PE, Mittermaier AK (2016) Rapid characterization of folding and binding interactions with thermolabile ligands by DSC. Chem Commun 52:13471–13474

Ilgu M, Nilsen-Hamilton M (2016) Aptamers in analytics. Analyst 141:1551–1568

Kim YS, Raston, N.H.A., Gu MB (2016) Aptamer-based nanobiosensors. Biosens Bioelectron 76:2–19

Lee JH, Pardi A (2007) Thermodynamics and kinetics for base-pair opening in the P1 duplex of the Tetrahymena group I ribozyme. Nucleic Acids Res 35:2965–2974

Lee JH, Juker F, Pardi A (2008) Imino proton exchange rates imply an induced-fit binding mechanism for the $VEGF_{165}$-targeting aptamer Macugen. FEBS Lett 582:1835–1839

Lee A-R, Cho SJ, Kim H-E, Lee Y-M, Lee J-H, Choi B-S (2012) NMR Study of hydrogen exchange in the DNA decamer duplexes containing the p53 response element. Bull Korean Chem Soc 33:685–688

Mascini M, Palchetti I, Tombelli S (2012) Nucleic acid and peptide aptamers: fundamentals and bioanalytical aspects. Angew Chem Int Ed 51:1316–1332

Neves MAD, Reinstein O, Saad M, Johnson PE (2010a) Defining the secondary structural requirements of a cocaine-binding aptamer by a thermodynamic and mutation study. Biophys Chem 153:9–16

Neves MAD, Reinstein O, Johnson PE (2010b) Defining a stem length-dependant binding mechanism for the cocaine-binding aptamer. A combined NMR and calorimetry study. Biochemistry 49:8478–8487

Neves MA, Blaszykowski C, Bokhari S, Thompson M (2015) Ultra-high frequency piezoelectric aptasensor for the label-free detection of cocaine. Biosens Bioelectron 72:383–392

Neves MA, Slavkovic S, Churcher ZR, Johnson PE (2017) Salt-mediated two-site ligand binding by the cocaine-binding aptamer. Nucleic Acids Res 45:1041–1048

Nonin S, Jiang F, Patel DJ (1997) Imino proton exchange and base-pair kinetics in the AMP-RNA aptamer complex. J Mol Biol 268:359–374

Nonin-Lecomte S, Lin CH, Patel DJ (2001) Additional hydrogen bonds and base-pair kinetics in the symmetrical AMP-DNA aptamer complex. Biophys J 81:3422–3431

Pei R, Shen A, Olah MJ, Stefanovic D, Worgall T, Stojanovic MN (2009) High-resolution cross-reactive array for alkaloids. Chem Commun 22:3193–3195

Reinstein O, Neves MAD, Saad M, Boodram SN, Lombardo S, Beckham SA, Brouwer J, Audette GF, Groves P, Wilce MCJ, Johnson PE (2011) Engineering a structure switching

mechanism into a steroid binding aptamer and hydrodynamic analysis of the ligand binding mechanism. BioChemistry 50:9368–9376

Reinstein O, Yoo M, Han C, Palmo T, Beckham SA, Wilce MCJ, Johnson PE (2013) Quinine binding by the cocaine-binding aptamer. Thermodynamic and hydrodynamic analysis of high-affinity binding of an off-target ligand. BioChemistry 52:8652–8662

Roncancio D, Yu H, Xu X, Wu S, Liu R, Debord J, Lou X, Xiao Y (2014) A label-free aptamer-fluorophore assembly for rapid and specific detection of cocaine in biofluids. Anal Chem 86:11100–11106

Sachan A, Ilgu M, Kempema A, Kraus G, Nilsen-Hamilton M (2016) Specificity and ligand affinities of the cocaine aptamer: impact of structural features and physiological NaCl. Anal Chem 88:7715–7723

Sharma AK, Heemstra JM (2011) Small-molecule-dependent split aptamer ligation. J Am Chem Soc 133:12426–12429

Slavkovic S, Altunisik M, Reinstein O, Johnson PE (2015) Structure-affinity relationship of of the cocaine-binding aptamer with quinine derivatives. Bioorg Med Chem 23:2593–2597

Stojanovic MN, de Prada P, Landry DW (2000) Fluorescent sensors based on aptamer self-assembly. J Am Chem Soc 122:11547–11548

Stojanovic MN, de Prada P, Landry DW (2001) Aptamer-based folding fluorescent sensor for cocaine. J Am Chem Soc 123:4928–4931

Vinkenborg JL, Karnowski N, Famulok M (2011) Aptamers for allosteric regulation. Nat Chem Biol 7:519–527

Zhang J, Jones CP, Ferre-D'Amare AR (2014) Global analysis of riboswitches by small-angle X-ray scattering and calorimetry. Biochem Biophys Acta 1839:1020–1029